Structural Engineering and Mechanics, Vol. 15, No. 6 (2003) 609-628
DOI: http://dx.doi.org/10.12989/sem.2003.15.6.609

Constitutive law for wedge-tendon gripping interface in anchorage device - numerical modeling and parameters identification

D. Marceau†

Department of Applied Sciences, Université du Québec à Chicoutimi, Quebec, Canada, G7H 2B1

M. Fafard† and J. Bastien†

Department of Civil Engineering, Laval University, Quebec, Canada, G1K 7P4

(Received June 12, 2002, Accepted March 4, 2003)

Abstract. Mechanical anchorage devices are generally tested in the laboratory and may be analyzed using the finite element method. These devices are composed of many components interacting through diverse contact interfaces. Generally, a Coulomb friction law is sufficient to take into account friction between smooth surfaces. However, in the case of mechanical anchorages, a gripping system, named herein the wedge-tendon system, is used to anchor the prestressing tendon. The wedge inner surface is made of a series of triangular notches designed to grip the tendon. In this particular case, the Coulomb law is not adapted to simulate the contact interface. The present paper deals with a new constitutive contact/gripping law to simulate the gripping effect. A parameter identification procedure, based on experimental results as well as on a finite element/neural network approach, is presented. It is demonstrated that all parameters have been selected in a satisfactory way and that the proposed constitutive law is well adapted to simulate the wedge gripping effect taking place in a mechanical anchorage device.

Key words: anchorage device; contact; finite element; neural networks; parameter identification; wedge-tendon interface.

1. Introduction

The prestressing technique has been used for many decades in the construction of new bridges and other types of structures. This technique is also used for the strengthening of existing bridges. In post-tensioned bridge structures, the tendons are stressed by means of jacks and they are anchored to the structure using mechanical anchorage devices. These devices are highly stressed because they alone must sustain the prestressing loads before the cement grout injection phase takes place. In external prestressing, the situation is even more critical because the anchorage mechanisms with the deviators are the only links between the structure and the tendons all during the structure's

† Professor

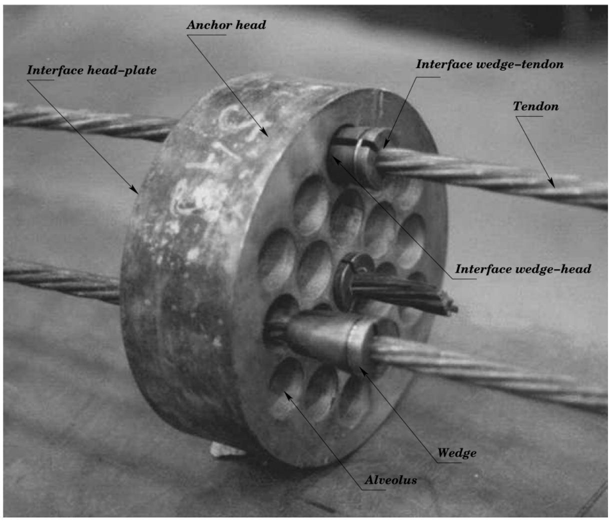

Fig. 1 Anchor head and contact interfaces

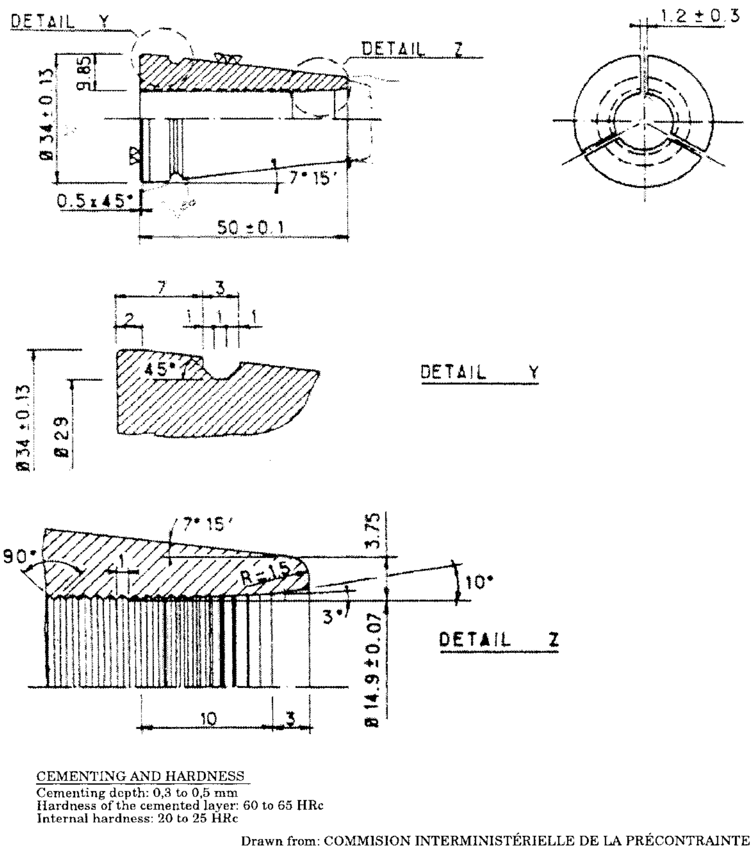

Fig. 2 Details of the wedge gripping devices

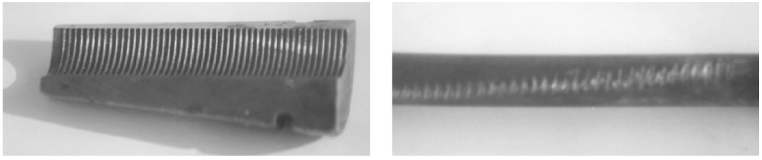

(a) Wedge (b) Tendon

Fig. 3 Notch prints of the wedge on the tendon

service life. The structure's security is thus strongly linked to the anchorage device's behaviour.

The development of these anchorage devices is, in general, done by specialized societies active in the prestressing construction field (Marceau 2001). The research and development programs of those societies are generally based on laboratory testing procedures and finite element analysis simulations. In order to perform reliable finite element analysis, the following requirements, among others, must be meet: adequate modeling of solids using an elasto-plastic constitutive law and a large strain approach, adequate modeling of the anchor head and plate contact interfaces, adequate modeling of the contact taking place between the jaws (composed of three wedges) and anchor head conic holes (see Fig. 1) and finally, adequate modeling of the contact interfaces occurring between tendons and wedges. In the two former cases, the surfaces are smooth and thus a classical contact approach with a Coulomb friction coefficient can be used. The wedge-tendon contact is however more complex due to the particulars of their contact surface. Fig. 2 gives the details of this surface where triangular notches are present to develop the wedge-tendon gripping action between the two components (wedge and tendon). Due to the conical form of the anchor head holes, the wedge triangular notches surrounding the tendon penetrate into the latter to grip it and therefore maintain it in place to develop prestress in the structures. In Fig. 3, one can observed the effect of triangular notches ("notchprint") on the tendon surface.

The literature on the finite element modeling of an anchorage device is very sparse. Some results on an axisymmetrical strand anchorage device using a geometrical simplification have been presented by Pecknold and Presswalla (1983). The authors eliminate the alveolus and made use of equivalent mechanical properties. No validation test has been presented in their paper. Bastien (1992) and Bastien *et al.* (1996) have performed some numerical simulation on three dimensional anchorage devices and the results have been compared to results produced in the laboratory. They used contact based on a node-to-node small relative displacement hypothesis. The wedge-tendon gripping action was considered to be such that the two components (wedge and tendon) may be assumed to act in a monolithic way. Therefore, the wedge-tendon assembly was replaced by a single truncated conical component. The latter had the same global dimensions as the wedge-tendon assembly and was meshed as such. Since the wedges are thin pieces submitted to a surface hardening fabrication process and since a tendon exhibits a linear elastic behaviour under service load conditions, the truncated conical components associated to the device are also considered to be linear elastic.

Recently, Marceau (2001) and Marceau *et al.* (2001a), have done a large number of simulations on anchorage devices of different geometrical shapes. The authors make use of a large strain, elasto-plastic constitutive law and large relative displacement contact elements. The wedge-tendon gripping action was considered to behave as described in Bastien (1992) for the study of multi-strand anchorage devices.

The aim this paper is to present a new approach to modeling the wedge-tendon interface base on experimental laboratory observations. This approach has been developed by Marceau (2001) and is quite different of the classical Coulomb friction law. The parameters of this constitutive law should be identified. In order to define the parameters of this new contact law, experimental test results, finite element results as well as a neural network approach have been combined (Marceau *et al.* 2001b, Henchi *et al.* 1998). It is the primary intent of this paper to present the experimental investigation performed on a mono-strand anchorage device, the results of which will serve as the basis for the new law development. The second aspect, a constitutive law calibration procedure necessary to identify its unknown parameters as well as its mathematical aspects is presented.

2. Experimental tests

The experimental test programs on large size anchorage devices are generally performed by specialized society in order to get an technical approval. These devices must undergo, with success, a series of experimental tests which are described in EOTA (2001). Briefly, the test consists in submitting the anchor device to a load corresponding to 80 percent of the ultimate strength of the tendons ($0{,}80F_u$). This load level represents the maximum prestressing force allowed at jacking, by many design codes (CAN/CSA-S6-88 1988, AASHTO 1994, BPEL 1990). The experimental test methodology described in the following paragraphs and applied to the mono-strand anchorage device has been based on the ETAG recommendations.

2.1 Description of the mono-strand anchorage device

In order to facilitate the experimental set-up design and procedure, a mono-strand anchorage device has been used (see Fig. 4) whose general dimensions can be found in Fig. 5. It can be observed that the alveolus forms an angle of 7,0º with respect to the anchorage's longitudinal axis while the wedge, designed to grip the tendon, forms an angle of 7,25º. A 15,7 mm diameter tendon have been used in the experiment. Tables 1 and 2 give the mechanical characteristics of each component of the anchorage device and of the tendon. It is assumed that all components have an elasto-plastic behaviour except for the wedge which is considered to remain elastic due to the surface hardness obtained through a special heat treatment.

Fig. 4 Mono-strand anchorage

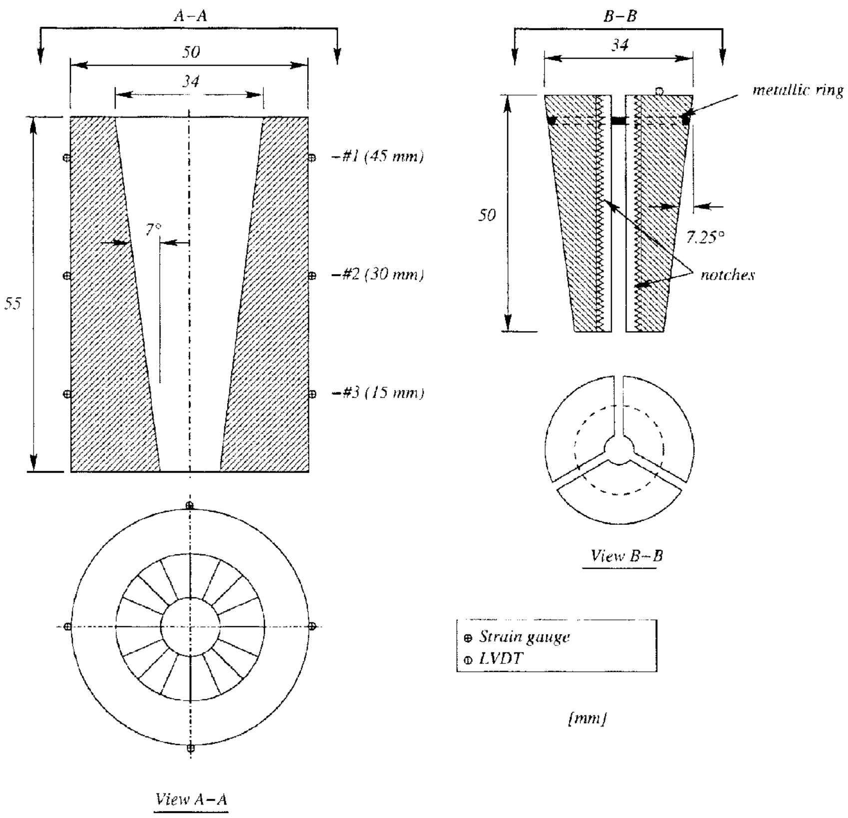

Fig. 5 Geometrical description of the anchorage device

Table 1 Mechanical properties of the anchorage device

Component	Yield limit (MPa)	Ultimate stress (MPa)	Strain at failure (%)
Anchor head	400	750	16
Anchor plate	260	400	22
Wedge[1]	400	Elastic behaviour	
Young modulus: $2,0 \cdot 10^5$ MPa, Poisson ratio: $0,30$			

Table 2 Characteristics of the tendon

Effective area (mm^2)	139
Nominal stress at failure (MPa)	1770
Nominal force at failure (kN)	246
Admissible stress (MPa) ($0,8 \cdot 1770$)	1416
Admissible stress (kN)	97
Young modulus: $2,0 \cdot 10^5$ MPa, Poisson ratio: 0,30	

2.2 Measurements

During loading, measurements such as displacements and strains have been taken. Strain gauges (±1 $\mu\varepsilon$) have been fastened at the periphery of the anchor head at three different levels to monitor the hoop strain (orthogonal to the loading direction) and the axial strain (parallel to the loading direction) as illustrated in Fig. 5. The relative penetration of the wedge into the alveolus hole has also been monitored using LVDTs (±0,01 mm) mounted at the top of the anchor head.

2.3 Loading

A bench test has been designed to load a mono-strand anchorage while stressing the tendon through the use of an hydraulic jack. The load was applied by step increments of 19,7 kN (corresponding to $0{,}1F_{rg}$, where F_{rg} = 197 kN = $0{,}8F_u$). The maximum load was maintained during 15 to 45 minutes and the unloading phase was performed using the same step pattern. The data was logged at each load step and, when maximum loading was reached, at five minute intervals. The complete procedure has been performed on five mono-strand anchorage devices.

2.4 Results

Tables 3 and 4 summarizes the experimental results. The wedge penetration results are presented for three different load levels corresponding to 25%, 60% and 100% of maximum loading respectively. Mean values where evaluated over the five experimental results. As far as strain results, Table 4 also presents mean values for different gauge locations (four gauges per height location) and covering the five experimental tests. Therefore, each mean value presented in Table 4 results from 20 experimental values. It is from these sets of values that maximum and minimum experimental results were extracted and presented in Table 4. It is assumed that the rather large range between minimum and maximum values, for a specific gauge level, is due to the jaw configuration and relative position inside the anchor head alveolus. As shown on Figs. 2, 4 and 5, the jaw is composed

Table 3 Penetration of the jaw in the anchor head for three load levels

Load (kN)	Penetration (mm)		
	Minimum	Mean	Maximum
49	0,68	1,25	1,61
123	1,60	2,56	3,10
196	2,70	3,79	4,43

Table 4 Strain at three different heights at maximum load level

Position	Axial strain ($\mu\varepsilon$)			Hoop strain ($\mu\varepsilon$)		
	Minimum	Mean	Maximum	Minimum	Mean	Maximum
1	−1225	−1754	−2436	2684	3417	5022
2	−724	−1041	−1154	1475	2629	3694
3	−515	−642	−817	679	849	1035

of three pieces attached together by a metallic ring. This ring allows a gap between the pieces in order for the jaw to adjust its configuration to the tendon presence. This adjustment results in non homogenous gap between the three pieces and therefore in non uniformed axial and hoop strains over the inner periphery of the anchor head alveolus at a given height. During the experimental testing, the relative position of the different jaw pieces relative to the gauges position was not recorded. It is the authors' opinion that the above phenomena is responsible for the result scattering.

2.5 General observations

Shape variation of the anchor head after loading indicates that permanent deformation has taken place. As far the wedges and tendon are concerned, it can be assumed that the wedge remains in its elastic behavior range due to the hardness of its surface while clearly, the tendon works in the elastic range based on the controlled load level during testing.

The relative displacement of the jaw with respect to the top of the anchor head is greatly influenced by the load level, the hoop rigidity of the anchor head and by the penetration of the wedge triangular notches into the tendon (gripping effect). We can observe this phenomenon on Fig. 3. Therefore, it may be assumed that at the beginning of loading, the "rigidity" of the interface is relatively soft and as the wedge penetrates the anchor head, i.e. as the notches penetrate the tendon, the rigidity of the interface increases. Theoretically, when all the notches have fully printed the tendon, no more penetration of the wedge surfaces into the tendon is possible.

In the axial direction, it may be assumed that no relative displacement exists between the tendon and the jaw due to the penetration of the triangular notches into the tendon. Finally, even if it is difficult to observe experimentally, it can be imagined that friction at the wedge-tendon interface in the circumference direction may take place.

All those general observations and remarks will be usefull to design a new wedge-tendon interface law.

3. Numerical finite element model

The mechanical behaviour of an anchorage device is complex. While being submitted to heavy prestressing loads, many phenomena can be observed: the wedge-tendon gripping action, the friction at the wedge-anchor head interfaces as well as at the anchor head-anchor plate interface, plastic strains and large relative displacements at some interfaces, to name a few. An adequate finite element model should be able to take into account all these mechanical phenomena.

In the present study, three types of non linearity have been taking into account: large strain (large displacement), plasticity and contact between some interfaces. In the latter, large relative displacement between interfaces has been considered using a slave-master concept (Marceau 2001, Laursen and Simo 1993). The penalty/augmented Lagrangian method has been used for the evaluation of the stresses at the different interfaces. This approach gives accurate results and allows non compatible meshes between different components of the anchor head. All mathematical and numerical techniques used for this model can be founded in Marceau (2001). The model has been tested and validated using literature information (Marceau 2001).

Based on the virtual work principle, the general variational equation used to express the large deformation frictional contact problem can be written as:

$$W(\delta\underset{\sim}{\varphi}, \underset{\sim}{\varphi}_t) = W_{int}(\delta\underset{\sim}{\varphi}, \underset{\sim}{\varphi}_t) + W_{ext}(\delta\underset{\sim}{\varphi}, \underset{\sim}{\varphi}_t) = 0 \tag{1}$$

where

$$W_{int}(\delta\underset{\sim}{\varphi}, \underset{\sim}{\varphi}_t) = \int_\omega \mathrm{tr}(\boldsymbol{\sigma}\delta\boldsymbol{D})d\omega \tag{2}$$

$$W_{ext}(\delta\underset{\sim}{\varphi}, \underset{\sim}{\varphi}_t) = W_v(\delta\underset{\sim}{\varphi}, \underset{\sim}{\varphi}_t) + W_\sigma(\delta\underset{\sim}{\varphi}, \underset{\sim}{\varphi}_t) \tag{3}$$

represent the internal and external contributions to the virtual work expressed on the deformed shape ω. In Eq. (2), $\boldsymbol{\sigma}$ and $\delta\boldsymbol{D}$ are respectively the Cauchy stress tensor and the strain rate tensor associated with the virtual displacement field $\delta\varphi$. On the other hand, Eq. (3) includes the virtual work produced by the applied forces $\underset{\sim}{f}_v$ on w and $\underset{\sim}{f}_\sigma$ on γ_σ such as:

$$W_v(\delta\underset{\sim}{\varphi}, \underset{\sim}{\varphi}_t) = -\int_\omega \delta\underset{\sim}{\varphi} \cdot \underset{\sim}{f}_v d\omega \tag{4a}$$

$$W_\sigma(\delta\underset{\sim}{\varphi}, \underset{\sim}{\varphi}_t) = -\int_{\gamma_\sigma} \delta\underset{\sim}{\varphi} \cdot \underset{\sim}{f}_\sigma d\gamma_\sigma \tag{4b}$$

As one can observe from Eq. (4b), it seems natural to split W_σ into two parts corresponding to the virtual work generated by the traction due to the frictional contact condition on $\gamma_c \in \gamma_\sigma$ and the prescribed forces applied on $\gamma_s \in \gamma_\sigma$. Therefore, Eq. (4b) can be rewritten as follows:

$$W_\sigma(\delta\underset{\sim}{\varphi}, \underset{\sim}{\varphi}_t) = W_s(\delta\underset{\sim}{\varphi}, \underset{\sim}{\varphi}_t) + W_c(\delta\underset{\sim}{\varphi}, \underset{\sim}{\varphi}_t) \tag{5}$$

with

$$W_s(\delta\underset{\sim}{\varphi}, \underset{\sim}{\varphi}_t) = -\int_{\gamma_s} \delta\underset{\sim}{\varphi} \cdot \underset{\sim}{f}_s d\gamma_s \tag{6a}$$

$$W_c(\delta\underset{\sim}{\varphi}, \underset{\sim}{\varphi}_t) = -\int_{\gamma_c} \delta\underset{\sim}{\varphi} \cdot \underset{\sim}{f}_c d\gamma_c \tag{6b}$$

defined in terms of $\underset{\sim}{f}_s$ and $\underset{\sim}{f}_c$ representing the prescribed forces and frictional contact traction respectively. The variational expression for the contact between different surfaces on the undeformed contact interface Γ_c^1 can be written (Marceau 2001) as:

$$W_c(\delta\underset{\sim}{\varphi}, \underset{\sim}{\varphi}_t) = \int_{\Gamma_c^1} [t_N \delta g + t_{T_\alpha} \delta\bar{\xi}^\alpha] d\Gamma_c^1 \tag{7}$$

where δg and $\delta\bar{\xi}^\alpha$ represent the virtual gap function and the parametric location of the projection of the slave particle on the master contact surface. t_N and t_{T_α} are the normal and tangential components of the nominal contact traction such that:

$$\underset{\sim}{t}^1(\underset{\sim}{X}^1, t) = t_N(\underset{\sim}{X}^1, t)\underset{\sim}{n}(\bar{\underset{\sim}{\xi}}, t) + t_{T_\alpha}(\underset{\sim}{X}^1, t)\underset{\sim}{\tau}^\alpha \tag{8}$$

where $\underset{\sim}{n}$ and $\underset{\sim}{\tau}^\alpha$ represent the normal and dual tangential basis vectors located at $\bar{\underset{\sim}{\xi}}$, the parametric projection point on the master contact surface. In the next section, we will present the contact relation necessary to estimated the normal and tangential stresses at the contact interfaces.

3.1 Contact constitutive laws

The contact interface between wedges and the inner part of an anchor head alveolus is based on the classical unilateral contact formulation coupled with the Coulomb friction law. Using a standard regularization technique, the mathematical problem can be summarized as follows:

$$\left.\begin{array}{ll} g(\underset{\sim}{X}^1, t) \le 0 & \\ t_N(\underset{\sim}{X}^1, t) \ge 0 & \text{with} \quad t_N = \varepsilon_N\langle g\rangle \\ t_N(\underset{\sim}{X}^1, t)g(\underset{\sim}{X}^1, t) = 0 & \end{array}\right\} \tag{9}$$

for the normal direction and

$$\left.\begin{array}{c} \Phi = \left\|\underset{\sim}{t}_T^\flat\right\| - \mu t_N \le 0 \\ \underset{\sim}{v}_T^\flat - \zeta\dfrac{\underset{\sim}{t}_T^\flat}{\left\|\underset{\sim}{t}_T^\flat\right\|} = \dfrac{1}{\varepsilon_T}L_v\underset{\sim}{t}_T^\flat \\ \zeta \ge 0 \\ \Phi\zeta = 0 \end{array}\right\} \tag{10}$$

in the tangential direction where ε_N and ε_T represent the penalty numbers associated with the regularization of the frictional contact problem. In Eq. (10), μ represents the friction coefficient, ζ the sliding rate and $L_v\underset{\sim}{t}_T^\flat$, the convected time derivative (Lie derivative) of the traction in the tangential space. Finally, $\langle\cdot\rangle$ is the Macauley bracket which defines the positive part of the operand.

For the wedge-tendon contact interface, a new contact law taking into account all the previous experimental observations is necessary. Firstly, the interface behaviour is considered orthotropic in the RTL directions. The normal contact stresses are assumed to act in the radial direction (R) while the longitudinal direction (L) is considered parallel to the tendon profile. While a Coulomb friction law is considered in the tangential direction (T), no relative displacement is assumed between the tendon and wedges in the longitudinal direction (L). Indeed in this direction, and contrary to the wedge-alveolus interface, the relative displacement is considered very small allowing for the present simplification. In the radial direction, an hyperbolic law is proposed and defined as (see Fig. 6):

$$t_R = \frac{\eta g_u}{g} \tag{11}$$

where η represents the stiffness in the radial direction and g, the actual radial distance between the wedge and the tendon such that:

$$g = g_0 - g_u \tag{12}$$

$$g_u = -\underset{\sim}{n} \cdot [\underset{\sim}{u}^1(\underset{\sim}{X}^1, t) - \underset{\sim}{u}^2(\underset{\sim}{\Psi}_0(\bar{\underset{\sim}{\xi}}), t)] \tag{13}$$

where g_0 defines the fictitious gap between the wedge and the tendon. The terms $\underset{\sim}{u}^1$ and $\underset{\sim}{u}^2$ represent the displacement field of the slave and master contact surfaces respectively.

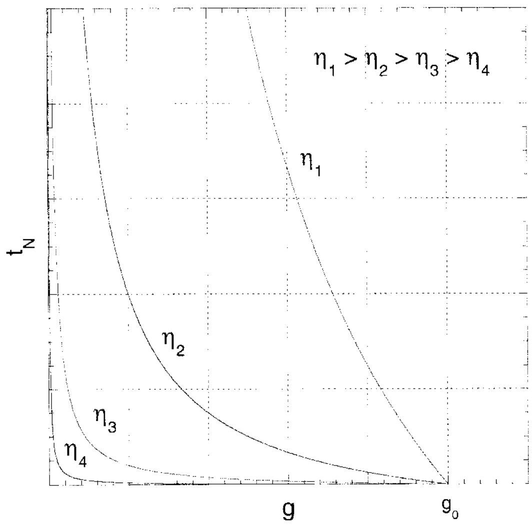

Fig. 6 Normal stress law for the wedge-tendon interface

The parameter g_0 can be associated with the depth of the notches. As seen on Fig. 6, for a given η value, when $g = g_0$ the radial stress is zero. At this point the notches begin to penetrate into the tendon and the stiffness increases progressively. When $g_u \rightarrow g_0$, the latter being the maximum allowed penetration, the radial stress increases rapidly. This radial stress will increase more or less rapidly depending on the value of η. Thus η and g_0 can be consider as unknown parameters needed to be identified.

From a mathematical point of view, the admissible conditions can be defined by:

$$\left.\begin{array}{c} g \geq 0 \\ g \leq g_0 \\ t_R \geq 0 \\ t_R(\underset{\sim}{X}^1, t) g(\underset{\sim}{X}^1, t) \geq 0 \end{array}\right\} \tag{14}$$

for the radial direction and

$$\left.\begin{array}{c} \Phi = \|t_{T_T}\| - \mu_{wt} t_R \leq 0 \\ \dot{\xi}^T - \zeta \dfrac{t_{T_T}}{\|t_{T_T}\|} = \dfrac{1}{\varepsilon_T} \dot{t}_{T_T} \\ \dot{\xi}^L = \dfrac{1}{\varepsilon_L} \dot{t}_{T_L} \\ \zeta \geq 0 \\ \Phi \zeta = 0 \end{array}\right\} \tag{15}$$

Table 5 Unknown parameters for the gripping/contact law

Parameter	Description	Sensitivity
η	Rigidity of the wedge notched-tendon interface along R direction	high
g_0	Maximum depth of the wedge notches	high
μ_{wh}	Friction coefficient at wedge-alveolus interface	high
μ_{wt}	Friction coefficient at wedge-tendon interface along T direction	low

for the longitudinal and tangential directions with μ_{wt}, $\dot{\bar{\xi}}^L$ and $\dot{\bar{\xi}}^T$, defining the Coulomb friction coefficient in the tangential direction and the wedge-tendon relative velocities in the corresponding directions. In the same manner, $\dot{t}_{T_L}$ and $\dot{t}_{T_T}$ represent the stress rate along the longitudinal and tangential directions respectively. The regularization is obtained using the penalty numbers ε_L and ε_T.

As described in Eq. (15), the Coulomb friction law is used in the tangential direction but not along the longitudinal direction for which no significant relative displacement occurs. In this case, a large penalty number can be used to simulate the perfect adhesive behaviour between the jaw and the tendon. Table 5 summarizes the unknown parameters to be identified.

3.2 Numerical techniques

This highly nonlinear problem has been solved using different numerical techniques. The arc-length controlled technique combined to the Newton-Raphson method have been used to linearize the problem. Due to large strain and contact phenomena, the resulting tangent stiffness matrix is non symmetric. Marceau (2001) presents the development to obtain this matrix resulting from a consistent linearization of Eq. (1).

This linearized system has been solved using an iterative method (preconditioned by BCGS). Contact interfaces were solved using a penalty coefficient of 10^5 in the normal and tangential directions using four Lagrangian augmentations. The numerical integration has been performed using a $3 \cdot 3 \cdot 3$ Gauss rule for hexahedron elements and a $3 \cdot 3$ Hammer-Gauss rule for triangular prismatic elements. For the contact interfaces, a $3 \cdot 3$ Gauss rule and three Hammer points have been used for quadrilateral and triangular elements respectively.

4. Identification using FEM and neural network

Identification of the different unknown parameters associated with the gripping/contact law has been performed with the combination of FEM and neural network methodologies. First, the range of each parameter is assessed. This may be done through a sensitivity analysis by comparing FEM numerical results with laboratory results.

Once the range of every unknown parameter is identified, each parameter range is cut in a certain number of intervals, N, to define $N + 1$ interval values. Then a finite element analysis is performed using all possible combinations of all the unknown parameter interval values. In this way a database is constructed by extracting numerical values of the FEM model at the anchorage locations where experimental results are recorded (see Fig. 7).

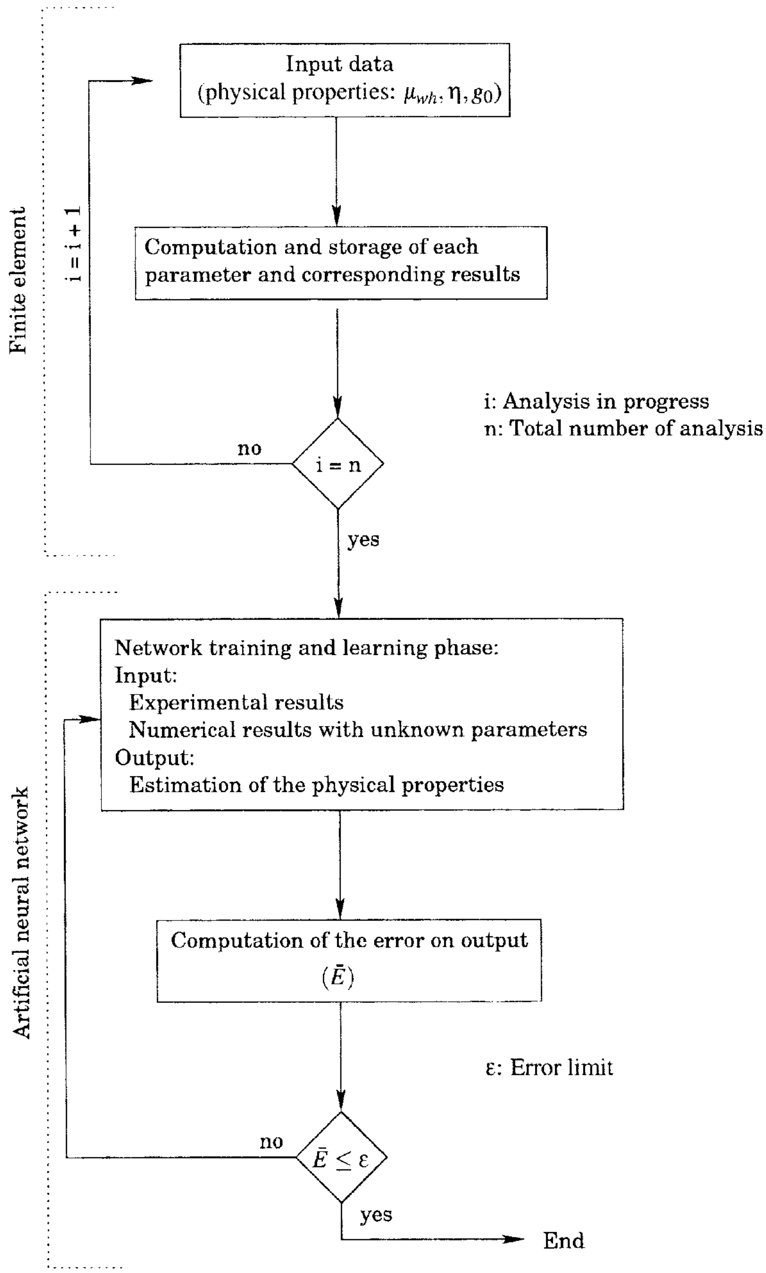

Fig. 7 FEM-Neural network identification procedure

This database is then used to proceed with the neural network software for what is commonly called “the learning phase”. Once this step is completed, experimental results may be introduced as input data in the neural network software, which has by now learned according to the database information, to predict the numerical values of the unknown parameters.

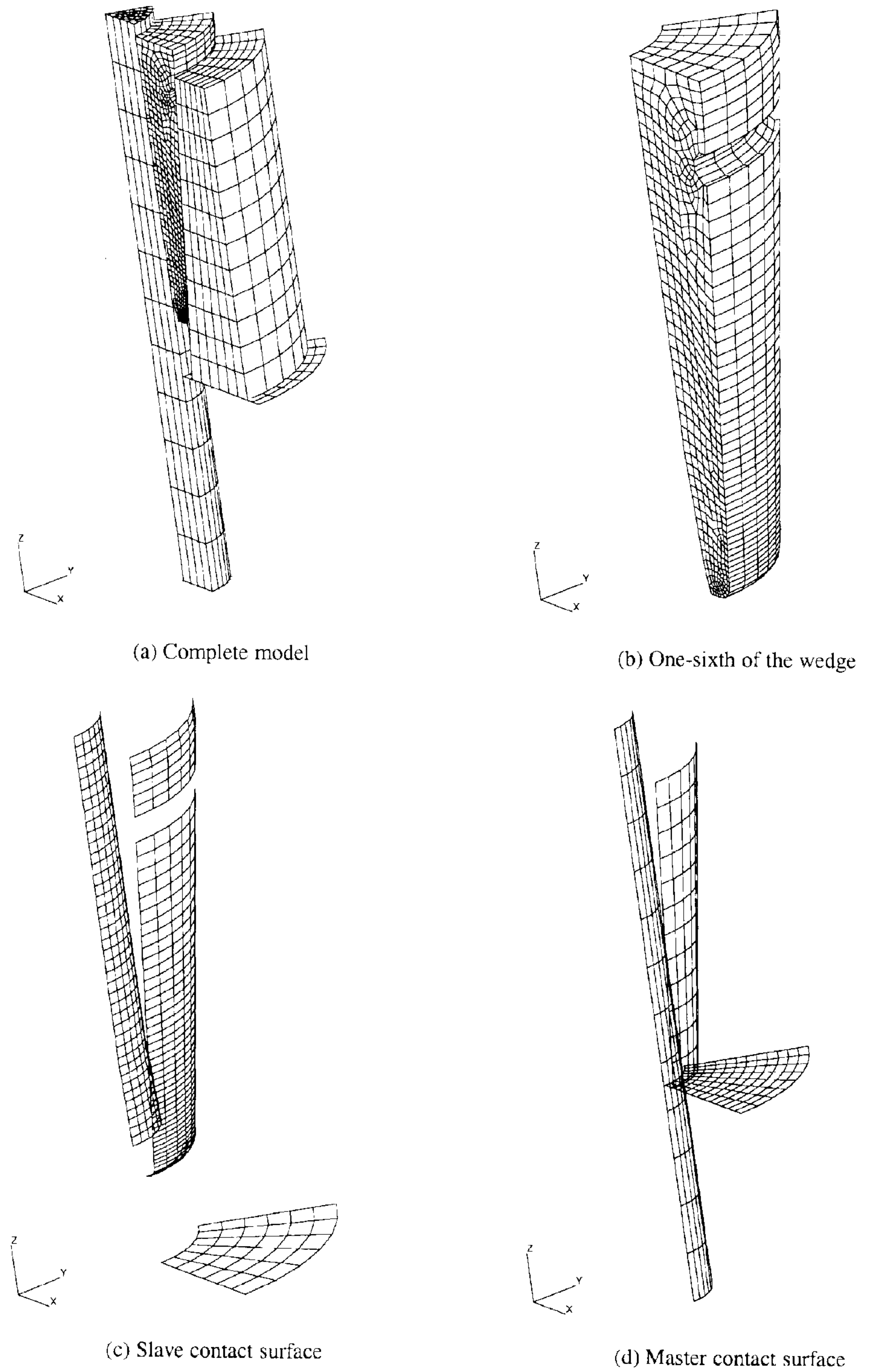

(a) Complete model

(b) One-sixth of the wedge

(c) Slave contact surface

(d) Master contact surface

Fig. 8 Mesh of the anchorage device

4.1 Finite element analysis and sensitivity study

Fig. 8, presents the finite element mesh of the LH1T15 anchorage device. Symmetry conditions have been taken into account for the analysis. Only one-sixth of the anchorage device was discretized. We can observe on Fig. 8(b) that all possible details of the wedge (see Fig. 2) have been taken into account except for the notches which have been modeled through the new proposed interface constitutive law named gripping/contact constitutive law. A total of 3828 elements and 4057 nodes have been used for a total of 12171 degrees of freedom. The load was directly apply to the end of the tendon by pulling it downwards.

The sensitivity analysis demonstrated that the friction coefficient between the wedge and the tendon in the T direction is not very important. Thus, it was fixed to 0,3. The same value was used for the contact between the bottom of the anchor head and the support.

Fig. 9 shows the influence of the three unknown parameters on the penetration of the wedge into the anchor head and on the axial strain comparing to experimental results. From this study, the lower and upper bounds of the parameters were established as follow:

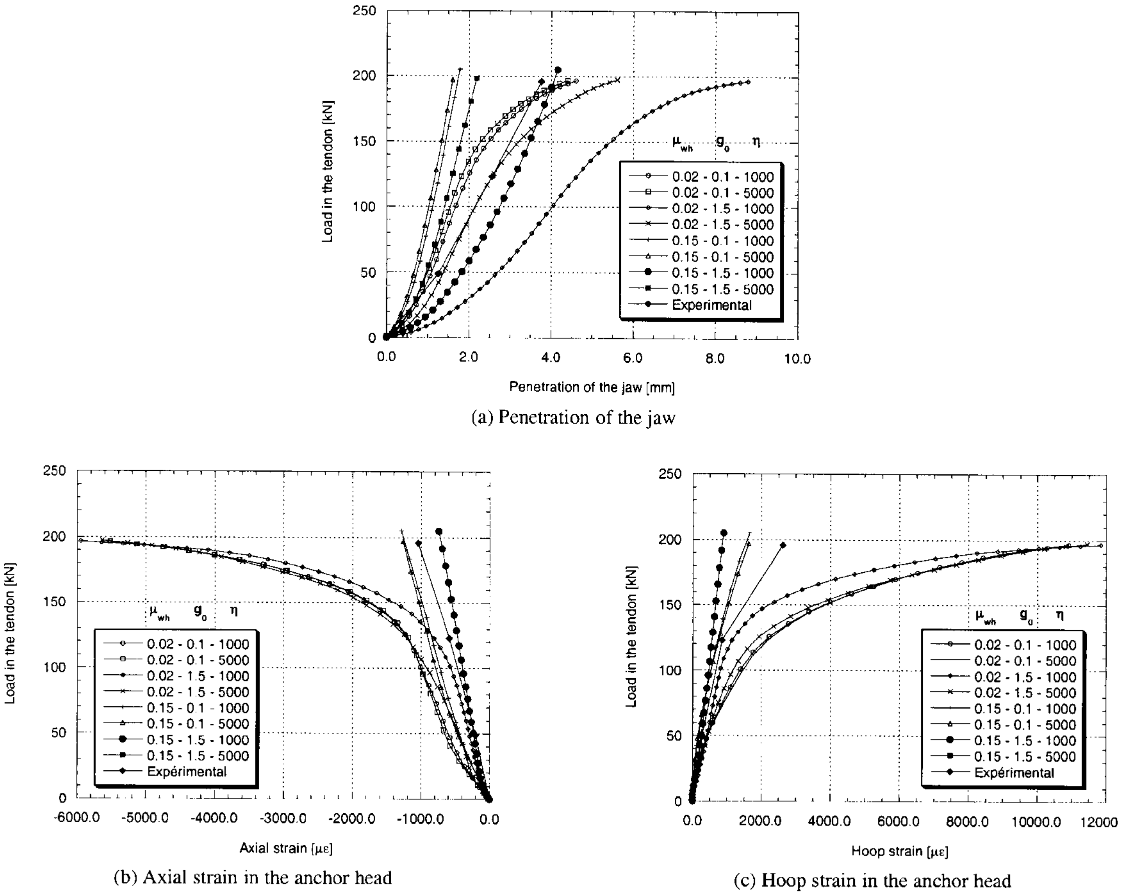

(a) Penetration of the jaw

(b) Axial strain in the anchor head

(c) Hoop strain in the anchor head

Fig. 9 Sensitivity analysis

$$\left.\begin{array}{ll} 1000 \le \eta \le 5000 & (\mathrm{MPa}) \\ 0{,}01 \le g_0 \le 1{,}5 & (\mathrm{mm}) \\ 0{,}02 \le \mu_{wt} \le 0{,}15 & \end{array}\right\} \tag{16}$$

4.2 Neural network calibration

Neural network represents a mathematical modeling of brain neuron network. It consists in transferring information through different layers of the network while adapting according to different external stimulations. The reader is refered to specialized literature to learn more about this subject (Langis 1997, Golden 1996).

The neural network being a modeling of a natural network, it should be able to adapt to a stimuli induced in the network and thus it should be composed of many neurons and layers as shown on Fig. 10. Normally each neuron of a layer is connected to all other neurons of the adjacent layers.

The first layer represents the external stimulation and it distributes the stimulus to the neurons of the second layers and so on. The last layer contain the target cells where the influx transmitted by the other layers are concentrated.

From a practical point of view, in the present case, the network input data at the first layer would be the laboratory results and the output the three unknown parameters (η, g_0, μ_{wt}). If the neural network has learned correctly, the output should be a good guess of those parameters for input data corresponding to the experimental results.

The learning phase was performed using the database containing the results from the FE analysis constructed with the combination of the unknown parameters. In the present case, since there are three unknown parameters, and since each unknown parameter range has been sliced in three (N = 3), 64 FE analysis ($(N+1)^3$) have been required to construct the database. From these 64 sets of numerical results, 54 sets were used to help the neural network learn. That is to say, numerical finite element results are introduced as neural network data input while each corresponding parameter combination is imposed as neural network output. By doing so, the neural network learns or adapts through what is called "weight functions".

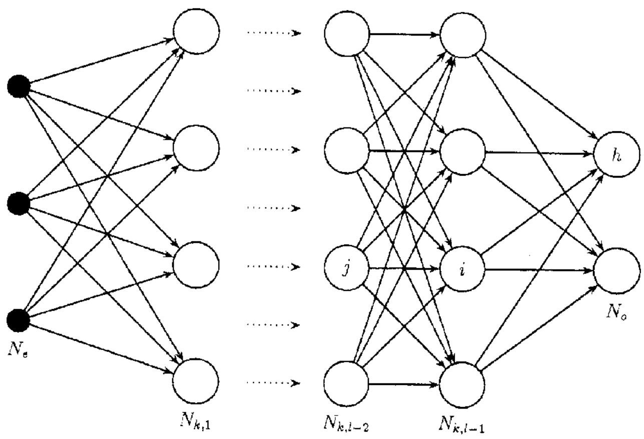

Fig. 10 Example of a neural network

Table 6 Results obtained for various neural network architecture

Architecture	Error (%)		η (MPa)	g_0 (mm)	μ_{wh}
	Learning	Validation			
9-12-3	3,9	8,4	3048	1,4887	0,0975
9-10-3	5,9	15,0	2982	1,5024	0,0805
9-6-3	4,9	12,3	4286	1,4831	0,0986
9-8-6-3	6,7	16,5	2005	1,5122	0,1003
9-10-8-3	4,0	8,4	2761	1,4955	0,09322
		Mean:	3016	1,4965	0,09402

Therefore, the learning phase is associated to a highly nonlinear process which one should see that it converges. In order to assure that convergence was reached, 10 sets of results from the data base were used. Numerical strains and wedge penetration results were introduced as data input in the neural network to predict the three unknown parameters. These neural network results were then compared to the values used in the first place to obtain the FEM numerical results.

Finally, when the neural network has learned enough (that is to say when convergence is reached), experimental results are introduced as input data to obtain an estimation of the parameters required to establish the gripping/contact constitutive law.

The utilization of a neural network software first requires its architecture definition in terms of the number of intermediate layers and number of neurons per layer. Table 6 summarizes results obtained from five different network configurations. The input layer of each configuration contains 9 neurons corresponding to the axial and hoop strains at three anchorage locations at maximum loading and wedge displacements at three different load levels. These values are respectively extracted from laboratory results in the final phase or from numerical results in the learning phase. The output layer of each configuration is composed of three neurons that are the unknown parameters: η, g_0, μ_{wt}.

As discussed before, due to the fact that the anchor jaw is herein made of three metallic pieces, the strain distribution is not uniform over the anchor head circumference. Since the relative position of the strain gauges to the jaw's metallic components was not recorded during the experimental investigation, a numerical weighted strain defined by the following equation was used in the present study:

$$\varepsilon = \frac{3(\varepsilon_0 + \varepsilon_{60}) + 6\varepsilon_{30}}{12} \tag{17}$$

where ε_0, ε_{60} and ε_{30} are the estimated strains at 0^o (free side), 30^o and 60^o (symmetry axis) respectively.

5. Comparison between calibrated model and test results

Making use of the mean values presented at the bottom of Table 6, it is now possible to analyze the mono-strand anchorage device and compare the numerical results with the experimental ones.

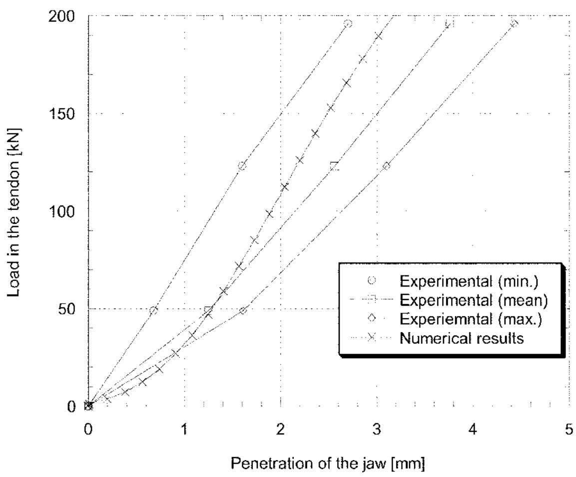

(a) Penetration of the wedge

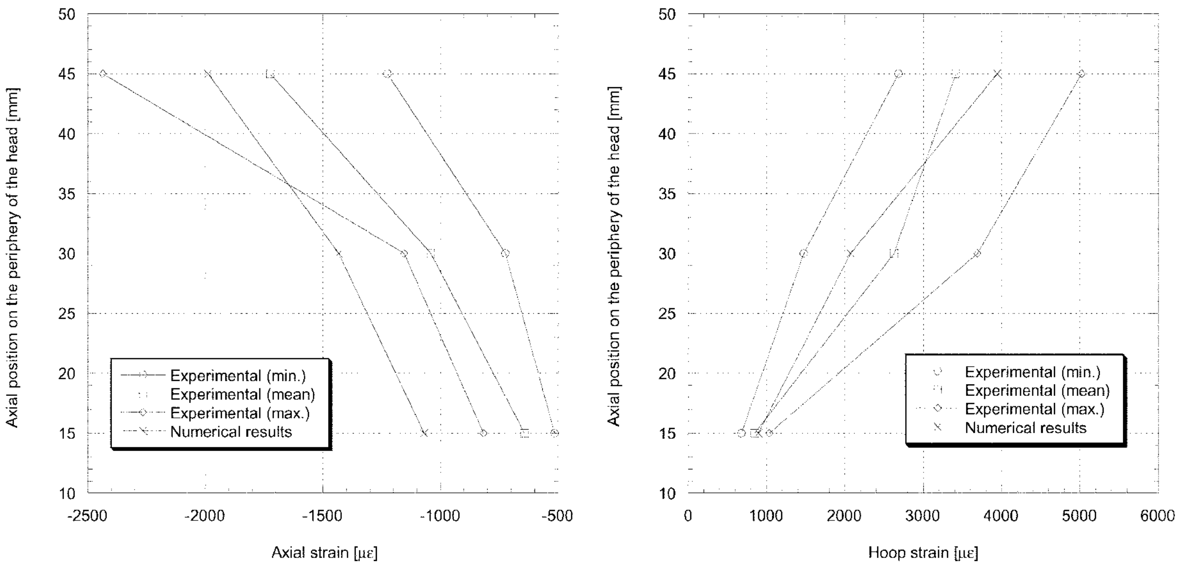

(b) Axial strain in the anchor head (c) Hoop strain in the anchor head

Fig. 11 Numerical results corresponding to the estimated parameters

Figs. 11(a) and 11(b) compare the wedge relative displacement and the hoop and axial anchor head strains together with the laboratory maximum, minimum and mean results. It is shown that the numerical results are generally bounded by the experimental ones and that they compare well with mean experimental values. However it is not the case for the numerical axial strains as they are outside the experimental range at the bottom periphery of the anchor head device. It is the opinion of the authors, that this situation occurs due to the jaw's geometric characteristic (three components) which generate a non symmetric axial strain distribution on the anchor head circumference, as discussed in the previous section, although it is calibrated as such by the neural network. The non

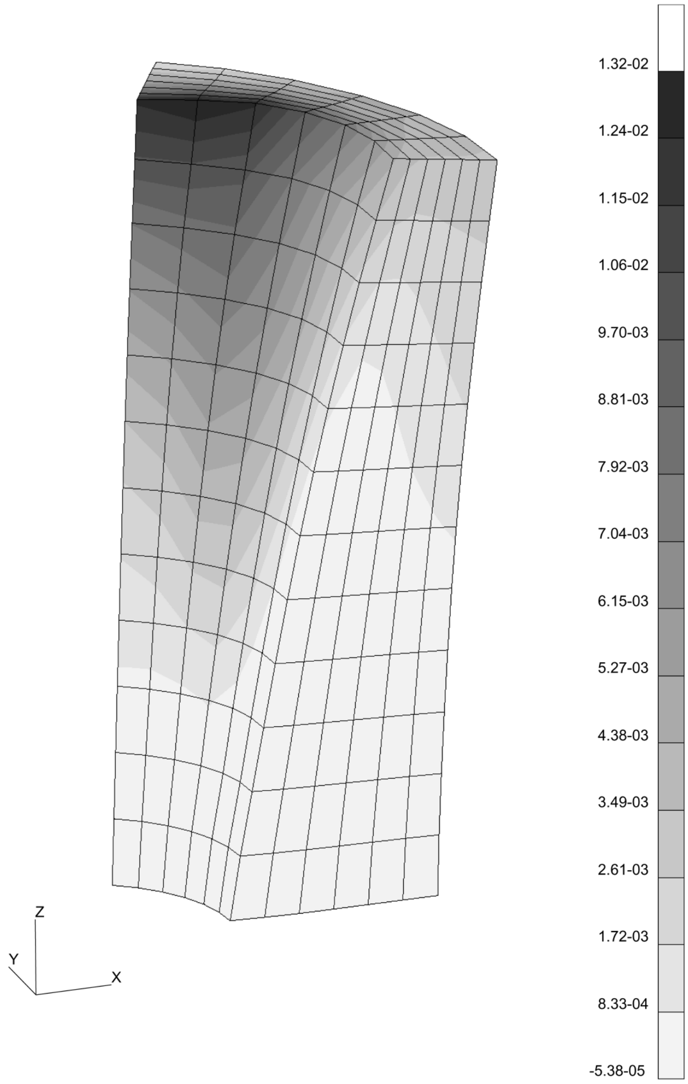

Fig. 12 Equivalent plastic strain on the deformed shape of the anchor head

symmetric strain distribution is well illustrated in Fig. 12 which presents the equivalent plastic strain distribution on the anchor head device's deformed shape.

6. Conclusions

In this paper a new constitutive law, the gripping/contact constitutive law, was presented in order to model contact between an irregular surface with triangular notches and a smooth surface. Based on results and observations obtain from a mono-strand anchorage devices experimental investigation, the proposed phenomenological approach permits to overcome the needs of a fine discretization of the interface which corresponds to a more complex and time consuming model.

The gripping/contact law (Eq. (15)) has been design based on results and observations relative to a mono-strand anchorage devices experimental investigation.

The estimation of the parameters of this constitutive law was done using a combination of finite element and neural network analysis. The estimated parameters obtained from this identification procedure were reintroduced into the FE model and compared to experimental test results. This comparison confirmed that the parameter estimations were very good. It is therefore concluded that for the FE analysis of multi-strand anchor head devices, which represents a higher level of complexity related to their geometric characteristics and number of contact interfaces, the developed gripping/contact law could be used with the following values : η = 3000 MPa, g_0 = 1,5 mm and μ_{wh} = 0,09. Of course, such parameters are adequate as far as the same tendon and wedge material are involved.

Acknowledgements

The authors would like to gratefully acknowledge the collaboration of Mr. Jean-Xavier Gartner, engineer student at the Ecole Catholique des Arts et Métiers, France. Partial support of this research by the Quebec Ministry of Transportation, the Natural Sciences and Engineering Research Council of Canada, and the Fonds québécois de la recherche sur la nature et les technologies, is also gratefully acknowledged.

References

AASHTO (1994), *AASHTO LRDF Bridge Design Specification*. American Association of State Highway and Transportation Officials. Section 5, U.S.A.

Bastien, J. (1992), "Comportement des têtes d'ancrage mono et multi-torons: Étude expérimentale et étude par éléments finis", Ph.D. thesis, Département de génie civil, Université Laval, Québec.

Bastien, J., Marceau, D., Fafard, M. and Chabert, A. (1996), "Experimental and numerical study of multi-strands wedge anchor heads", In "*Post-Tensioned Concrete Structures*", **2**, 695-704. The Concrete Society, 3 Eatongate, 112 Windsor Road, Slough, SL1 2JA.

BPEL (1990), *Règles techniques de conception et de calcul des ouvrages et constructions en béton précontraint suivant la méthode des états limites.* Marché public des travaux. Fascicule no. 5, Cahier des clauses générales, France.

CAN/CSA-S6-88 (1988), *Calcul des ponts-routes, Une norme Nationale du Québec.* Association Canadienne de normalisation, Ont. Canada.

EOTA (2001), *Guideline for European Technical Approval of Post-tensioning Kits for Prestressing of Structures*. EOTA, Brussels. Draft version, 139 pages.

Golden, R.M. (1996), *Mathematical Methods for Neural Network Analysis and Design*. Bradford Books, first edition.

Henchi, K., Fafard, M., Talbot, M. and Langis, D. (1998), "L'application des réseaux neuronaux artificiels pour l'identification et la détection de l'endommagement dans les ponts", Revue européenne des éléments finis, **7**, 257-272.

Langis, D. (1997), "Identification structurale et réseaux neuromimétiques: calibration de modèles éléments finis", Master's thesis, Département de génie civil, Université Laval, Québec.

Laursen, T.A. and Simo, J.C. (1993), "A continuum-based finite element formulation for the implicit solution of multibody, large deformation frictional contact problem", *Int. J. Num. Meth. Engng*., **36**, 3451-3485.

Marceau, D. (2001), "Modélisation du contact tridimensionnel en grands déplacements relatifs et son application à l'étude des dispositifs d'ancrages multitorons", Ph.D. thesis, Département de génie civil, Université Laval, Québec.

Marceau, D., Bastien, J., Fafard, M. and Chabert, A. (2001a), "Experimental and numerical studies of mono-strand anchorage", *Int. J. Struct. Eng. Mech.*, **12**(2), 119-134.

Marceau, D., Fafard, M., Bastien, J. and Boudjelal, M. (2001b). "Application des réseaux neuromimétiques la détermination du comportement déformationnel d'un dispositif d'ancrage multitorons", In "*Actes du cinquième colloque en calcul des structures*", **1**, 189-196. Ed. Batoz, Ben Dhi & Chauchot (Tecknea, Toulouse), Giens, France.

Pecknold, D.A. and Presswalla, H.H. (1983), "Elastoplastic analysis of thick perforated plates with application to prestressing anchor head", *Comput. Struct.*, **20**(4), 539-553.